ANALYTICAL AND NUMERICAL EVALUATION OF COUPLED GALLOPING OF SLENDER TOWERS

Liang Wu and Delong Zuo
Department of Civil, Environmental and Construction Engineering, Texas Tech University
Lubbock, TX, USA

ABSTRACT: Many previous studies have been conducted to study galloping of slender structures or structural components. While some recent studies have investigated the problem of coupled galloping involving the across-wind and along-wind vibrations, few of these investigations focused on the prediction of the steady-state amplitudes of coupled galloping oscillations. This paper presents a state-space formulation of the equations of motion for the analysis of coupled translational galloping of full-scale structures under the quasi-steady assumption. A numerical procedure based on the Fourth-order Runge-Kutta method is used to solve these equations of motion and predict coupled galloping amplitudes. A full-scale tower which has been observed to exhibit coupled galloping is used as an example structure to illustrate the application of the proposed analytical-numerical formulation.

Keyword: Slender tower, coupled galloping, state-space formulation.

1. INTRODUCTION

Galloping is a type of wind-induced low-frequency oscillation due to negative aerodynamic damping that can reach high-amplitudes. This type of vibration frequently occurs for slender structures with cylindrical structural members of bluff cross-sections. For example, iced power transmission lines, highway lighting poles, and bridge hangers have been observed to gallop at excessive amplitudes in natural winds.

Early study of the galloping phenomenon focused on the across-wind vibration and neglected the oscillation in the along-wind direction as well as torsional motion. Based on the quasi-steady assumption, Den Hartog [1] introduced a criterion for across-wind galloping that specifies the condition under which a conductor will gallop. This criterion has been widely used to assess the propensity of a variety of cross-sectional shapes to gallop in the across-wind direction (e.g., [2-6]) based on force coefficients obtained from wind tunnel tests. To predict the across-wind galloping amplitude of bluff cylinders, Parkinson and Smith [7] formulated a nonlinear differential equation that governs the across-wind galloping motion of a single-degree-of-freedom oscillator by expressing the aerodynamic force coefficients as polynomial functions of the vibration velocity. They solved this equation for the steady-state vibration amplitude using the Krylov-Bogoliubov method. On the basis of this formulation, Novak [8] investigated the influence of the slope of the lateral force coefficient at zero angle of attack (i.e., positive, zero and negative) on the galloping response, revealing the possibility of the translational galloping even when the Den Hartog criterion is not satisfied. Using an example of a prism that is stable in smooth flow but unstable in turbulent flow, he also pointed out that the effect of turbulence on the galloping instability should not be neglected. Subsequently, Richardson [9, 10] proposed an alternative method for the prediction of across-wind galloping amplitude. Although this method is still based on the principle of energy balance, it expresses the lateral force coefficient as a Fourier series instead of a polynomial function.

Following the early studies of across-wind galloping, more recent studies have taken into account vibrations in more than one direction. Jones [11] derived a coupled galloping criterion for a two-degree-of-freedom system with oscillations in both the across-wind and along-wind directions. However, Jone's study only addressed the situation where the along-wind direction coincides with one of the principal axes of the structure and the natural frequencies of the modes in the directions of the two principal axes are identical. Liang et al. [12] developed a seemingly more general formula to calculate the onset wind velocity for coupled

[+1]isfa0001@jaxa.jp, [+2]isfa0002@company.com, [+3]isfa0003@univ.ac-u.jp

translational galloping without the restriction of the wind direction., Li et al. [13] further extended the formulation by Liang et al. [12] to enable the prediction of steady-state amplitudes of coupled translational galloping. However, these studies incorrectly asserted that the translational oscillations in the two orthogonal directions are in phase. This led to the erroneous conclusion that coupled translational galloping occurs only when the natural frequencies of a structure in the two principal translational directions are the same.

In a recent investigation, Nikitas and Macdonald [14] conducted a comprehensive review of the galloping instability criteria and modeled coupled translational galloping without restrictions on the natural frequencies and the wind direction. They further investigated the effect of detuning between the natural frequencies of a structure in the principal directions on the trajectory of the galloping oscillation. However, this investigation of the vibration trajectory is trivial because the formulation of coupled galloping model was based on the linearization of the aerodynamic force coefficients and thereby is only suitable for small vibration amplitude, which is often not of interest. In order to accurately predict the steady-state trajectory of the galloping oscillation, the nonlinear aerodynamic damping has to be properly modeled.

In this paper, the aerodynamic damping in the two translational directions are expressed as polynomial functions of the velocities, and the equations of motion for coupled translational galloping are formulated in a state-space form under the quasi-steady assumption. Then the steady-state amplitudes of the coupled galloping oscillations are evaluated by solving the state-space equations of motion with the Fourth-order Runge-Kutta method. As an illustration, the proposed approach is used to assess the galloping oscillation of a slender tower.

2. ANALYTICAL-NUMERICAL FORMULATION

For slender structures under wind excitation, the torsional response can be neglected. In this situation, with the quasi-steady assumption, the instantaneous flow and displacement quantities for a section of unit length can be represented by Figure 1. In this graph, $\bar{U}$ is the mean along-wind speed, u and v are the along-wind and across-wind components of the turbulence, $\bar{r}_x$ and $\bar{r}_y$ are the mean displacements of the section in the directions of the principal axes, r_x and r_y are the corresponding dynamic displacements, D and L are the drag and lift forces, respectively, $\bar{\alpha}$ is the angle of incidence of the mean wind component defined relative to the principle axis x, $\Delta\alpha$ is the increment of the angle of incidence of the total horizontal wind speed relative to the cross-section, the magnitude of which is U_{rel}, and α is the total angle of incidence of the relative wind speed.

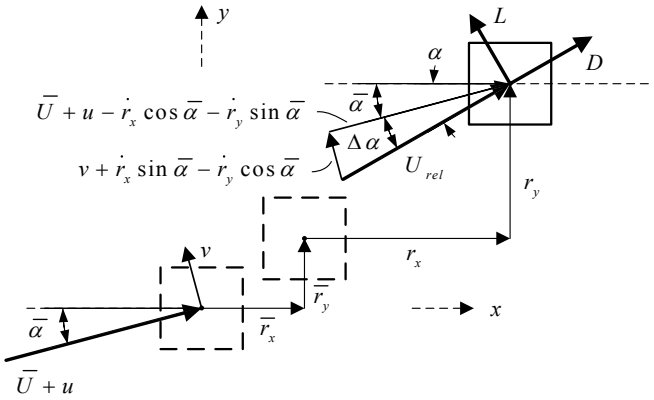

Figure 1 Instantaneous wind and displacements in two translational degrees of freedom

The instantaneous drag and lift forces acting on the segment of unit length can be expressed as

$$\begin{bmatrix} D & L \end{bmatrix}^T = \left[\frac{1}{2}\rho U_{rel}^2 B C_D(\alpha) \quad \frac{1}{2}\rho U_{rel}^2 B C_L(\alpha) \right]^T \tag{1}$$

in which $C_D(\alpha)$ and $C_L(\alpha)$ are the drag and lift force coefficients measured at the angle of incidence α.

The attack-angle-dependent force coefficients can be approximated by polynomials of the attack angle as:

$$\begin{bmatrix} C_D(\alpha) & C_L(\alpha) \end{bmatrix}^T = \left[\sum_{j=1}^{m} A_i \alpha^j \quad \sum_{j=1}^{n} B_j \alpha^j \right]^T \tag{2}$$

in which A_j and B_j are the coefficients of the polynomials approximating the drag and lift force coefficients, respectively.

Since $u \ll \bar{U}$ and $v \ll \bar{U}$, $\Delta\alpha$ and U_{rel}^2 in Figure 1 and equation (1) can be expressed as

$$\Delta\alpha = \arctan\left(\frac{v + \dot{r}_x \sin\bar{\alpha} - \dot{r}_y \cos\bar{\alpha}}{\bar{U} + u - \dot{r}_x \cos\bar{\alpha} - \dot{r}_y \sin\bar{\alpha}} \right) \tag{3}$$

$$\begin{aligned} U_{rel}^2 &= [(\bar{U}+u)\cos\bar{\alpha} - \dot{r}_x - v\sin\bar{\alpha}]^2 + [(\bar{U}+u)\sin\bar{\alpha} - \dot{r}_y + v\cos\bar{\alpha}]^2 \\ &\approx \bar{U}^2 + 2u\bar{U} - 2\left[(\bar{U}+u)\cos\bar{\alpha} - v\sin\bar{\alpha}\right]\dot{r}_x - 2\left[(\bar{U}+u)\sin\bar{\alpha} + v\cos\bar{\alpha}\right]\dot{r}_y + \dot{r}_x^2 + \dot{r}_y^2 \end{aligned} \tag{4}$$

The drag and lift forces can be decomposed into the components along the principal axes, the resultants of which are

$$\begin{bmatrix} f_x \\ f_y \end{bmatrix} = \begin{bmatrix} \cos\alpha & -\sin\alpha \\ \sin\alpha & \cos\alpha \end{bmatrix} \begin{bmatrix} D \\ L \end{bmatrix} \tag{5}$$

Substituting equation (1) into equation (5), the equations of motion of a segment of unit length can be expressed as

$$\mathbf{m}\ddot{\mathbf{r}} + \mathbf{c}\dot{\mathbf{r}} + \mathbf{m}\boldsymbol{\Omega}^2\mathbf{r} = \mathbf{f} \tag{6}$$

where,

$$\mathbf{r} = \begin{bmatrix} r_x & r_y \end{bmatrix}^T;\ \mathbf{f} = \begin{bmatrix} f_x & f_y \end{bmatrix}^T = \frac{1}{2}\rho U_{rel}^2 B \begin{bmatrix} C_D\cos\alpha - C_L\sin\alpha & C_D\sin\alpha + C_L\cos\alpha \end{bmatrix} \tag{7}$$

$$\mathbf{m} = \begin{bmatrix} m & 0 \\ 0 & m \end{bmatrix};\ \mathbf{c} = \begin{bmatrix} c_{xx} & 0 \\ 0 & c_{yy} \end{bmatrix};\ \boldsymbol{\Omega}^2 = \begin{bmatrix} \omega_x^2 & 0 \\ 0 & \omega_y^2 \end{bmatrix} \tag{8}$$

Assuming that the vibration of a slender tower is dominated by one mode each in the directions of the principle axes, the translational displacements of a slender tower at a height of z above ground can be expressed as

$$\mathbf{r} = \boldsymbol{\Phi}(z)\mathbf{q}(t) \tag{9}$$

in which the modal matrix and the generalized coordinate vector are

$$\boldsymbol{\Phi}(z) = \begin{bmatrix} \phi_x(z) & 0 \\ 0 & \phi_y(z) \end{bmatrix};\ q(t) = \begin{bmatrix} q_x(t) \\ q_y(t) \end{bmatrix} \tag{10}$$

With equation (9), the generalized equations of motion for a slender tower of height h take the form

$$\mathbf{M}\ddot{\mathbf{q}} + \mathbf{C}\dot{\mathbf{q}} + \mathbf{M}\boldsymbol{\Omega}^2\mathbf{q} = \mathbf{F} \tag{11}$$

where,

$$\mathbf{M} = \int_0^h \left(\boldsymbol{\Phi}^T \mathbf{m} \boldsymbol{\Phi} \right) dz = \begin{bmatrix} M_x & 0 \\ 0 & M_y \end{bmatrix} \tag{12}$$

$$\mathbf{C} = \int_0^h \left(\boldsymbol{\Phi}^T \mathbf{c} \boldsymbol{\Phi} \right) dz = \begin{bmatrix} C_{xx} & 0 \\ 0 & C_{yy} \end{bmatrix} \tag{13}$$

$$\mathbf{F} = \int_0^h \left(\boldsymbol{\Phi}^T \mathbf{f} \right) dz = \left[\int_0^h \phi_x f_x dz \quad \int_0^h \phi_y f_y dz \right]^T = \begin{bmatrix} F_x & F_y \end{bmatrix}^T \tag{14}$$

The elements of the above matrices are given by

$$M_x = \int_0^h m(z)\phi_x^2(z)dz;\ M_y = \int_0^h m(z)\phi_y^2(z)dz \tag{15}$$

$$C_{xx} = \int_0^h c_{xx}\phi_x^2(z)dz = 2M_x\omega_x\zeta_x;\ C_{yy} = \int_0^h c_{yy}\phi_y^2(z)dz = 2M_y\omega_y\zeta_y \tag{16}$$

$$F_x = \int_0^h \frac{1}{2}\rho U_{rel}^2 B\phi_x \left(C_D\cos\alpha - C_L\sin\alpha \right) dz;\ F_y = \int_0^h \frac{1}{2}\rho U_{rel}^2 B\phi_y \left(C_D\sin\alpha + C_L\cos\alpha \right) dz \tag{17}$$

in which ζ_x and ζ_y are the damping ratios of the two modes considered.

Ignoring the buffeting forces for the galloping analysis, $\Delta\alpha$ and U_{rel}^2 in equations (3) and (4) can be further simplified as

$$\Delta\alpha = \frac{\phi_x \dot{q}_x \sin\bar{\alpha} - \phi_y \dot{q}_y \cos\bar{\alpha}}{\bar{U} - \phi_x \dot{q}_x \cos\bar{\alpha} - \phi_y \dot{q}_y \sin\bar{\alpha}} \tag{18}$$

$$U_{rel}^2 = \bar{U}^2 - 2\phi_x \dot{q}_x \bar{U}\cos\bar{\alpha} - 2\phi_y \dot{q}_y \bar{U}\sin\bar{\alpha} + \phi_x^2 \dot{q}_x^2 + \phi_y^2 \dot{q}_y^2 \tag{19}$$

Because C_D and C_L are functions of α and $\alpha = \bar{\alpha} + \Delta\alpha$, the generalized equations of motion (11) are nonlinearly coupled differential equations with the generalized coordinates in the denominator. In the following, a numerical method is used to evaluate the amplitudes of coupled galloping oscillations.

First, the generalized equations of motion (11) are rewritten in a state-space form

$$\dot{\boldsymbol{\eta}} = \mathbf{A}\boldsymbol{\eta} + \mathbf{B}\mathbf{F}_\mathbf{b} \tag{20}$$

where

$$\boldsymbol{\eta} = \begin{bmatrix} q_x & q_y & \dot{q}_x & \dot{q}_y \end{bmatrix}^T;\ \mathbf{F}_\mathbf{b} = \begin{bmatrix} 0 & 0 & F_x & F_y \end{bmatrix}^T \tag{21}$$

$$\mathbf{A} = \begin{bmatrix} 0 & 0 & 1 & 0 \\ 0 & 0 & 0 & 1 \\ -\omega_x^2 & 0 & -2\omega_x\zeta_x & 0 \\ 0 & -\omega_y^2 & 0 & -2\omega_y\zeta_y \end{bmatrix};\ \mathbf{B} = \begin{bmatrix} 0 & 0 & 0 & 0 \\ 0 & 0 & 0 & 0 \\ 0 & 0 & 1/M_x & 0 \\ 0 & 0 & 0 & 1/M_y \end{bmatrix} \tag{22}$$

The fourth-order Runge-Kutta method is used to solve the above system of first-order differential equations. Because the differential equations are coupled, the solution for the coupled galloping oscillations is obtained iteratively. The general form of equation (20) can be expressed as

$$\dot{\boldsymbol{\eta}} = \mathbf{f}(t, \boldsymbol{\eta}^T) \tag{23}$$

in which,

$$\mathbf{y} = \boldsymbol{\eta} = \begin{bmatrix} \eta_1 & \eta_2 & \eta_3 & \eta_4 \end{bmatrix};\ \mathbf{f} = \begin{bmatrix} f_1(t,\boldsymbol{\eta}^T) & f_2(t,\boldsymbol{\eta}^T) & f_3(t,\boldsymbol{\eta}^T) & f_4(t,\boldsymbol{\eta}^T) \end{bmatrix}^T \tag{24}$$

The iterative steps of the fourth-order Runge-Kutta method for solving equation (20) are as follows

$$\mathbf{K}_1 = h\mathbf{f}(t_i, \boldsymbol{\eta}_i^T) \tag{25}$$

$$\mathbf{K}_2 = h\mathbf{f}\left(t_i + 0.5h, (\boldsymbol{\eta}_i + 0.5\mathbf{K}_1)^T\right) \tag{26}$$

$$\mathbf{K}_3 = h\mathbf{f}(t_i + 0.5h, (\boldsymbol{\eta}_i + 0.5\mathbf{K}_2)^T) \tag{27}$$

$$\mathbf{K}_4 = h\mathbf{f}\left(t_i + h, (\boldsymbol{\eta}_i + \mathbf{K}_3)^T\right) \tag{28}$$

$$\boldsymbol{\eta}_{i+1} = \boldsymbol{\eta}_i + \frac{1}{6}\left(\mathbf{K}_1 + 2\mathbf{K}_2 + 2\mathbf{K}_3 + \mathbf{K}_4\right) \tag{29}$$

where i is the iteration step, and

$$h = t_{i+1} - t_i;\ \boldsymbol{\eta}_i = \begin{bmatrix} \eta_{1i} & \eta_{2i} & \eta_{3i} & \eta_{4i} \end{bmatrix}^T \tag{30}$$

$$\mathbf{K}_j = \begin{bmatrix} K_{1j} & K_{2j} & K_{3j} & K_{4j} \end{bmatrix}^T, j = 1,2,3,4 \tag{31}$$

The analytical-numerical solution of the coupled galloping problem will be illustrated by a full-scale application example in the following section.

3. EXAMPLE APPLICATION

As an illustrative example, the analytical-numerical method developed herein is used to evaluate the galloping oscillation of a full-scale slender tower at the field testing site at Texas Tech University.

Figure 2 shows the tower consisting of a base tube and a swing tube, both being rectangular Hollow Structural Steel sections. The base tube is rigidly connected to the foundation, and the swing tube pivots about the top of the base tube. When in the upright position, the swing tube is pinned to the base tube approximately 0.9 m above the foundation. Also shown in Figure 2 are the coordinate system for describing wind-induced

vibration of the tower. U and α in this system are the wind speed and wind angle of incidence, respectively. Overbar represents time averaging.

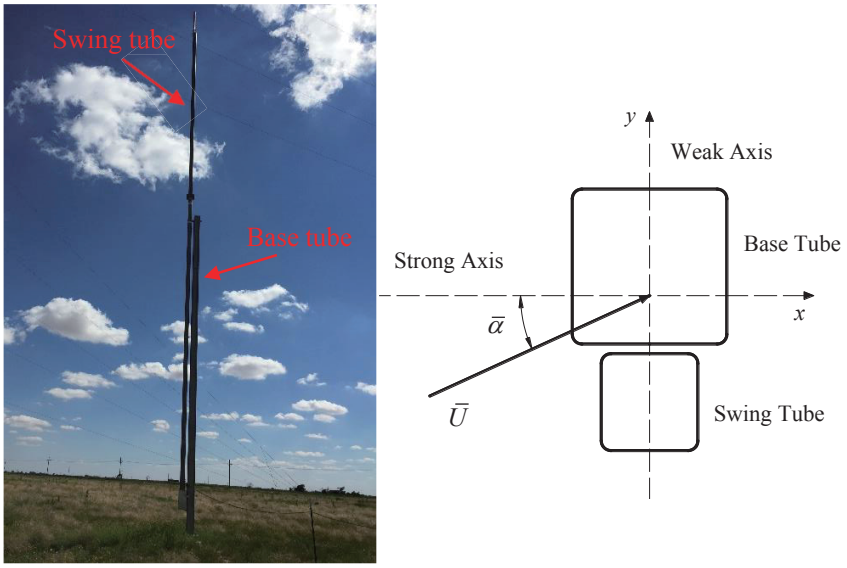

(a) (b)

Figure 2 (a) A tilt tower for positive train control and (b) coordinate system for description of wind and vibration

The major structural properties of the tower are given in Table 1. Based on measurements of the ambient vibration of the tower using accelerometers, the fundamental frequencies of the structure about the weak and strong axes are approximately 0.62 Hz and 0.7 Hz, respectively, and the damping ratios of the fundamental modes about these two axes are approximately 1.5% and 1.4%, respectively.

Table 1 Dimensions of the structural members of the tower instrumented for vibration measurements

	Width (cm)	Wall Thickness (cm)	Corner Radius/Width	Length (m)
Base Tube	21.0	0.74	0.07	9.3
Swing Tube	12.7	0.59	0.09	16.5

Assessment of the galloping stability of the tower requires information about the mode shapes of the structure, the mean wind speed profile along the height, as well as the drag and lift force coefficients of the cross-sections. For this illustrative example, only the fundamental modes in the two principal axes are considered. The shapes of these two modes are estimated through a finite-element model of the structure using the commercial software ANSYS. These numerically obtained mode shapes are then fitted to two third-order polynomial functions, the results of which are

$$\phi_x(z) = 1.102\times10^{-4}z^3 - 6.253\times10^{-4}z^2 + 0.0274z;\quad \phi_y(z) = 7.777\times10^{-4}z^3 + 1.5399\times10^{-4}z^2 + 0.0241z \quad (32)$$

The mean wind speed profile at the site of the tower is assumed to follow the power law

$$\bar{U}(z) = \bar{U}_{ref}\left(\frac{z}{z_{ref}}\right)^{\beta} \quad (33)$$

in which $\bar{U}_{ref}$ is the mean wind speed at the reference height z_{ref}, chosen at the top of the tower; β is the power law exponent. According the wind speed measurements at heights of 2.44 m, 10 m and 18 m by anemometers on an adjacent tower, the mean value of the power exponent β at this site is approximately 0.2.

The drag and lift force coefficients of the different segments of the tower are taken as the drag and lift force coefficients of the corresponding section models tested in a series of wind tunnel experiments described in [15]. Since the wind tunnel experiments suggest that the wind loading of the tower segments is not significantly affected by the Reynolds number, the force coefficients obtained at a test wind speed of 10 m/s are

used herein. Using a formulation described in [16], it is determined that for this structure, galloping instability can occur only when $0° < |\bar{\alpha}| < 9°$ or $81° < |\bar{\alpha}| < 90°$. The largest $\Delta\alpha$ during vibration is assumed to be smaller than 9°. Then in the ranges of $-18° < |\alpha| < 18°$, $-99° < \alpha < -72°$ and $72° < \alpha < 99°$, the aerodynamic force coefficients are approximated by 5th order polynomials of the wind angle of incidence.

As an illustration, Figure 3 shows drag and lift force coefficients of the section of the tower consisting of both the base tube and the swing tube (C_{D1} and C_{L1}) and the those of the section of the tower consisting of only the swing tube (C_{D2} and C_{L2}) as well as the polynomial approximations of these coefficients. It can be seen that the force coefficients of the swing tube section are well approximated by the corresponding polynomials. However, the polynomial fit for the force coefficients of the section consisting of both the base and swing tubes are not very satisfactory near some wind angles of incidence. However, the effect of this misfit is expected to be insignificant as the wind speeds over this section of the tower is lower than those over the section consisting of the swing tube only and for the mode shapes of interest, the displacement of the lower section is smaller than that of the upper section.

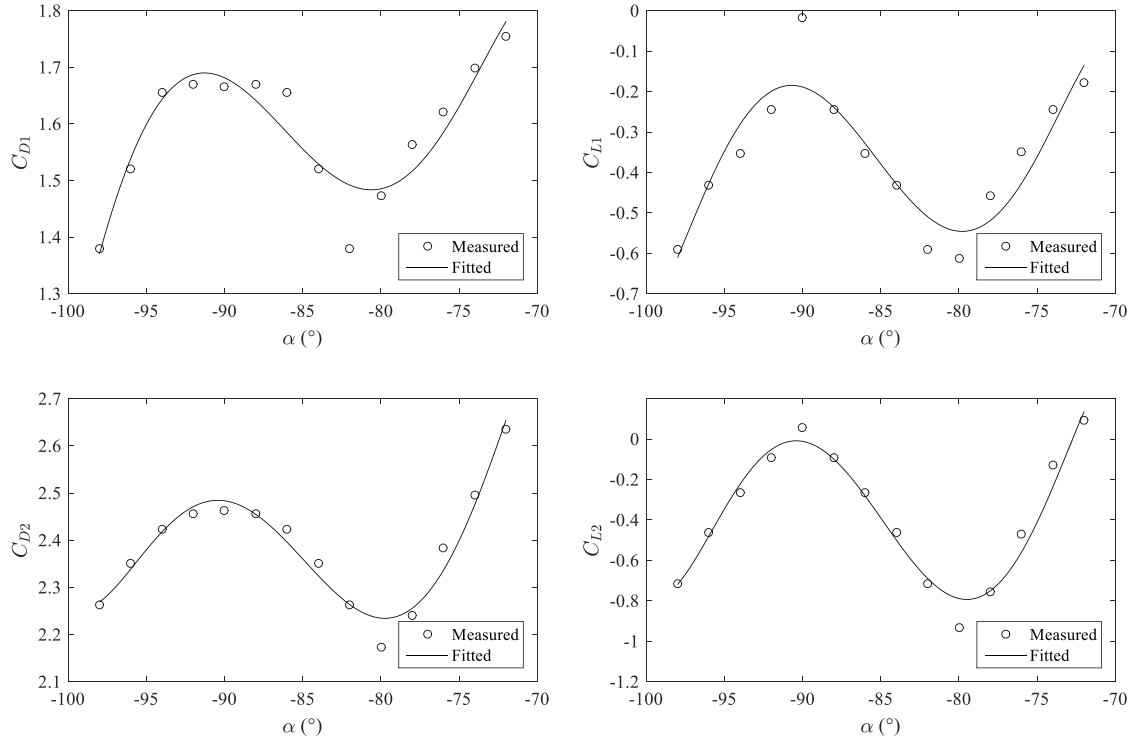

Figure 3 Aerodynamic force coefficients of the slender tower sections

Using the analytical-numerical formulation described above, the responses of the tower to winds of various speeds and angles of incidence are evaluated. As an example, Figure 4 shows the displacement time histories at the top of the slender tower for a mean wind speed of $\bar{U} = 18$ m/s at the top of the tower and a mean angle of incidence of $\bar{\alpha} = -85°$. The initial conditions used in the numerical evaluations are 0.01 m dynamic displacements and zero velocities at the top of the tower in the directions of both the weak and the strong axes, and the time step used in the numerical evaluation is 0.01 s. It can be seen that under this wind condition, the coupled galloping vibration is dominated by the component about the weak axis (i.e., in the *x*-direction), but vibration of significant amplitude also occurred about the strong axis (i.e., in the *y*-direction).

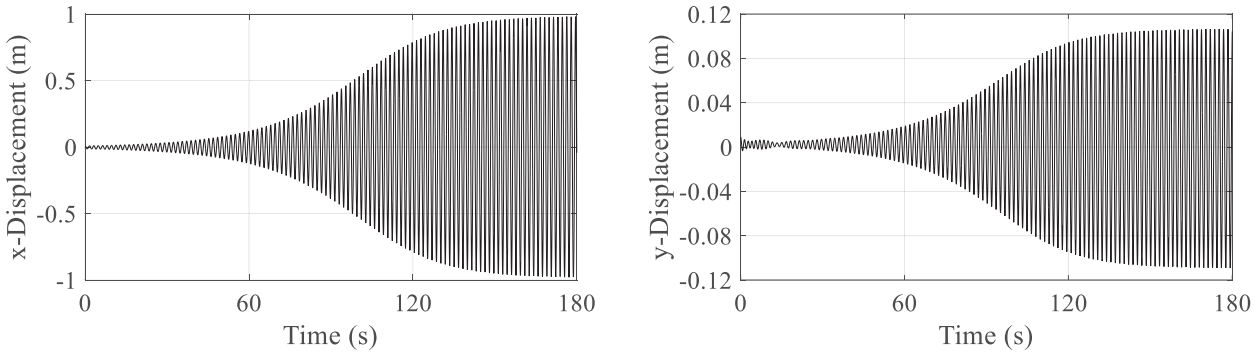

Figure 4 Simulated time histories of coupled galloping oscillation at $\bar{U}=18$ m/s and $\bar{\alpha}=-85°$

The coupling between the vibration components about the weak and strong axes also manifests itself in the vibration frequencies of these components. Figure 5 shows the frequencies of the vibration components depicted in Figure 4, which are estimated by identifying the peaks in the wavelet scalograms of the displacements [17] computed using the complex Morlet wavelet. It is evident that while the frequencies of the components about the principal axes are distinct at the beginning, when the vibration amplitudes are small, they quickly converge and become essentially identical when the vibration amplitude about the weak axis becomes large. This feature of the coupled galloping oscillation has also been observed in the recorded oscillation of the full-scale tower. For example, Figure 6 shows the displacement time histories of the full-scale tower dominated by the component about the weak axis and the corresponding time histories of the instantaneous dominant vibration frequencies, which are also estimated by identifying the peaks in the wavelet scalograms of the displacements. As in the case of the numerical simulation, the frequencies of the two vibration components are distinct when the amplitude of the vibration about the weak axis is small but converge when the amplitude of the vibration about the weak axis is large.

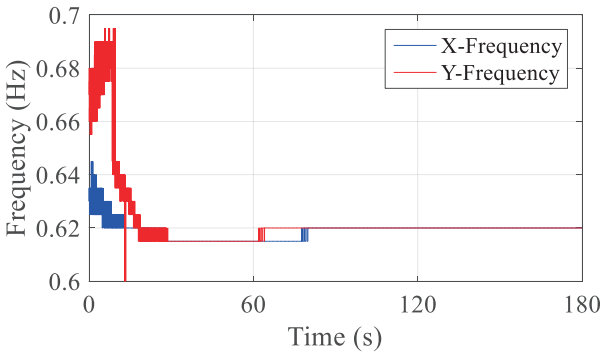

Figure 5 Evolution of vibrations frequencies of simulated coupled galloping oscillation

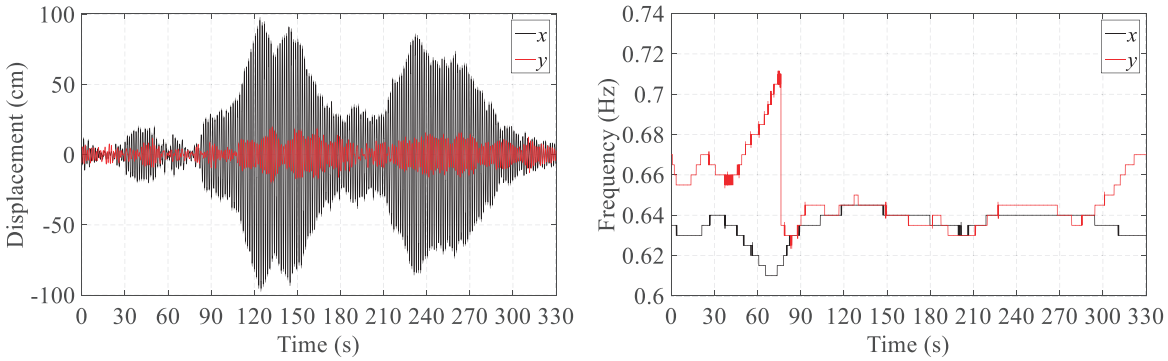

Figure 6 Evolution of vibration frequencies with displacement amplitudes for vibration of full-scale tower dominated by the component about the weak axis

In addition to producing results that reveal characteristics of the coupled galloping similar to those

observed in the full-scale data, the analytical-numerical formulation is also able to effectively predict the overall dynamic behavior of the tower at a given combination of wind speed and wind angle of incidence. Figure 7 shows the steady-state amplitudes of the coupled galloping oscillation of the full-scale tower predicted using the analytical-numerical formulation over ranges of mean wind speed and angle of incidence, and Figure 8 shows the measured 10-min maximum displacements of the tower about its principal axes over corresponding mean wind speed and direction. It can be seen that the analytical-numerical model successfully predicts the wind speed and direction range over which large-amplitude coupled galloping occurs. Direct comparison of the predicted vibration amplitudes to the measured vibration amplitudes is challenging because full-scale winds are often nonstationary with changing mean wind speed and direction. However, according to Figure 7 and Figure 8, the analytical-numerical method can indeed approximately predict some largest-amplitude oscillations (e.g., those at wind angles of incidence of about 90°).

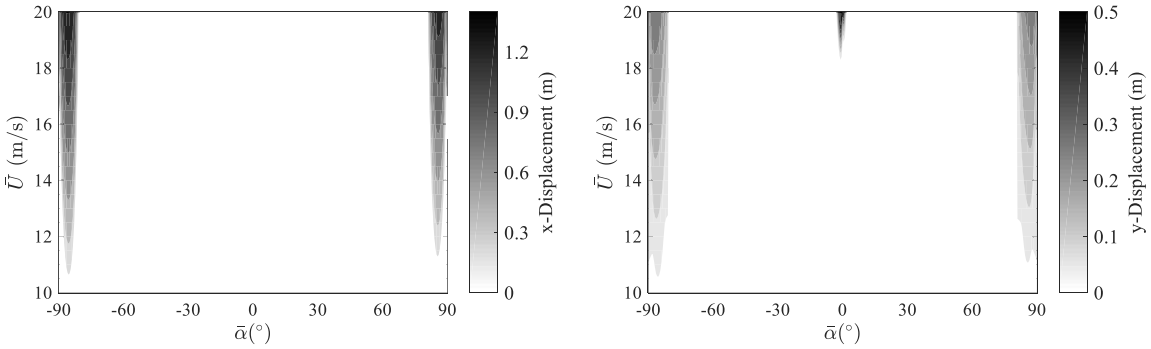

Figure 7 Numerically predicted vibration amplitudes

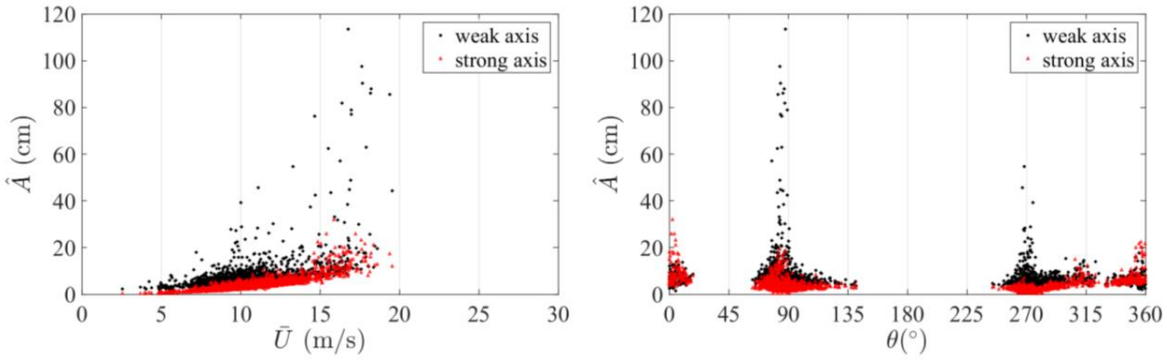

Figure 8 Measured maximum displacements

4. Conclusion

Under excitation from wind, slender towers with certain cross-sectional shapes can be susceptible to galloping oscillations. This paper presents the formulation of an analytical model in terms of a state-space equation that can be used to evaluate coupled galloping of a slender tower. Because the equation of motion involves nonlinear coupling, the Runge-Kutta method is used to yield numerical solutions. For illustration, the proposed method is used to evaluate the coupled galloping of a full-scale tower. Comparison between the numerical results and the measured vibrations of the full-scale tower suggests that the proposed method can effectively capture the essential characteristics of the full-scale coupled oscillations.

REFERENCES

1) Den Hartog, J.P., *Transmission line vibration due to sleet.* transactions of the american institute of electrical engineers, 1932. 51(4): p. 1074–1086.
2) Novak, M., H. Tanaka, and A.G. Davenport, *Vibration of towers due to galloping of iced cables.* ASCE Journal of the Engineering Mechanics Division, 1978. 104(2): p. 457-473.

3) Nigol, O. and P.G. Buchan, *Conductor Galloping Part I - Den Hartog Mechanism.* Power Apparatus and Systems, IEEE Transactions on, 1981. PAS-100(2): p. 699-707.
4) Norberg, C., *Flow around rectangular cylinders: Pressure forces and wake frequencies.* Journal of Wind Engineering and Industrial Aerodynamics, 1993. 49(1–3): p. 187-196.
5) Reuther, J.J., et al., *Constrained multipoint aerodynamic shape optimization using an adjoint formulation and parallel computers, Part 1.* Journal of Aircraft, 1999. 36(1): p. 51-60.
6) Reuther, J.J., et al., *Constrained multipoint aerodynamic shape optimization using an adjoint formulation and parallel computers, Part 2.* Journal of Aircraft, 1999. 36(1): p. 61-74.
7) Parkinson, G.V. and J.D. Smith, *The Square Prism as an Aeroelastic Non-linear Oscillator.* Quarterly Journal of Mechanics and Applied Mathematics, 1964. XVII Pt. 2: p. 225-239.
8) Novak, M., *Galloping Oscillations of Prismatic Structures.* ASCE Journal of the Engineering Mechanics Division, 1972. 98(EM1): p. 27-46.
9) Richardson, A., *Predicting Galloping Amplitudes: II.* Journal of Engineering Mechanics, 1988. 114(11): p. 1945-1952.
10) Richardson, A., *Predicting Galloping Amplitudes.* Journal of Engineering Mechanics, 1988. 114(4): p. 716-723.
11) Jones, K.F., *Coupled vertical and horizontal galloping.* Journal of Engineering Mechanics, ASCE, 1992. 118(1): p. 92-107.
12) Liang, S., et al., *An evaluation of onset wind velocity for 2—D coupled galloping oscillations of tower buildings.* Journal of Wind Engineering and Industrial Aerodynamics, 1993. 50(0): p. 329-339.
13) Li, Q.S., J.Q. Fang, and A.P. Jeary, *Evaluation of 2D coupled galloping oscillations of slender structures.* Computers & Structures, 1998. 66(5): p. 513-523.
14) Nikitas, N. and J. Macdonald, *Misconceptions and Generalizations of the Den Hartog Galloping Criterion.* Journal of Engineering Mechanics, 2014. 140(4): p. 04013005.
15) Zuo, D., D.A. Smith, and S.M. Morse, *Coupled galloping of a slender tower with distinct natural frequencies in two orthogonal directions: experimental study*, in *14th International Conference on Wind Engineering*. 2015: Porto Alegre, Brazil.
16) Wu, L. and D. Zuo. *Coupled galloping of a slender tower with distinct natural frequencies in two orthogonal directions: analytical study*. in *14th International Conference on Wind Engineering*. 2015. Porto Alegre, Brazil.
17) Kijewski, T. and A. Kareem, *Wavelet Transforms for system identification in civil engineering.* Computer-aided Civil and Infrastructure Engineering, 2003. 18: p. 339-355.